Structure and electronic structure evolution of P2-NaxCoO2 phases from X-ray diffraction and 23Na magic angle spinning nuclear magnetic resonance

Yohan Biecher, Anthony Baux, François Fauth, Claude Delmas, Gillian R. Goward, Dany Carlier

Structure and electronic structure evolution of P2-Na_xCoO_2 phases from XRD and ^{23}Na MAS NMR

Yohan Biecher[a], Anthony Baux[a], Francois Fauth[b], Claude Delmas[a], Gillian R. Goward[b], Dany Carlier[a*]

[a]*CNRS, Univ. Bordeaux, Bordeaux INP, ICMCB UMR 5026, F-33600 Pessac, France*

[b]*CELLS - ALBA synchrotron, Cerdanyola del Vallès, E-08290 Barcelona, Spain*

[c]*Department of Chemistry & Chemical Biology, McMaster University, Hamilton, Ontario L8S 4M1, Canada*

* *Corresponding author: dany.carlier@icmcb.cnrs.fr*

Abstract : P2-$Na_{0.70}CoO_2$ is considered as a model material for positive electrode application in Na-ion batteries. In this paper, we report an in-depth study and characterization of P2-Na_xCoO_2 system, in order to understand the material evolution from the point of view of structure at different scales and electronic properties upon charge up to high voltage (4.6 V). Using a combination of ex-situ and operando XRD and ex situ ^{23}Na MAS NMR we discuss the structural changes occurring due to the deintercalation of Na^+ ions from the interlayer slabs and the change in the electronic structure and magnetic properties. The XRD study allows discussing the general evolution in relation with previous works. The novelty lies here in the observation for the first time of an ordered phase for x=1/3 appearing between above 4.3 V followed by a disordering in the slabs stacking for higher voltages. The combination of the data obtained by the different techniques allowed the interpretation of the NMR shift and shape evolution versus the Na content. This study reveals a complex behavior due to the presence of localized and delocalized electrons whose relative proportions is changing versus Na content.

Introduction

Layered colbaltates oxides have been investigated for their application as positive electrode in Li-ion or Na-ion batteries[1–6] and are often considered as model compounds. These lamellar oxides consist of a stacking of edge-sharing MO_6 octahedra layers forming MO_2 slabs between which alkali ions are intercalated. Whereas the lithium ions are in octahedral sites, the sodium ones can be found either in octahedral sites, like in O3-$NaCoO_2$[7] or in prismatic sites for lower sodium contents, like in P2-Na_xCoO_2, P3-Na_xCoO_2[6] and P'3-$Na_{2/3}Mn_{1-y}Fe_yO_2$[8,9]. Following the nomenclature developed by Delmas *et al.*[10], the P2 stacking of Na_xCoO_2 phases consists in an alternation of CoO_2 slabs formed by edge-sharing CoO_6 octahedra and interslab spaces in which x Na^+ ions can be located in two prismatic sites (**Figure 1a**) : one sharing edges (Na_e) and one sharing faces (Na_f) with the surrounding CoO_6 octahedra (**Figure 1b**). Due to large Na^+-Na^+ electrostatic in-plane repulsion, the sodium ions tend to order in the interslab space, yielding a very complex phase diagram as investigated by some of us using *in-situ* X-ray Diffraction (XRD) for $0.45 < x < 0.9$[11].

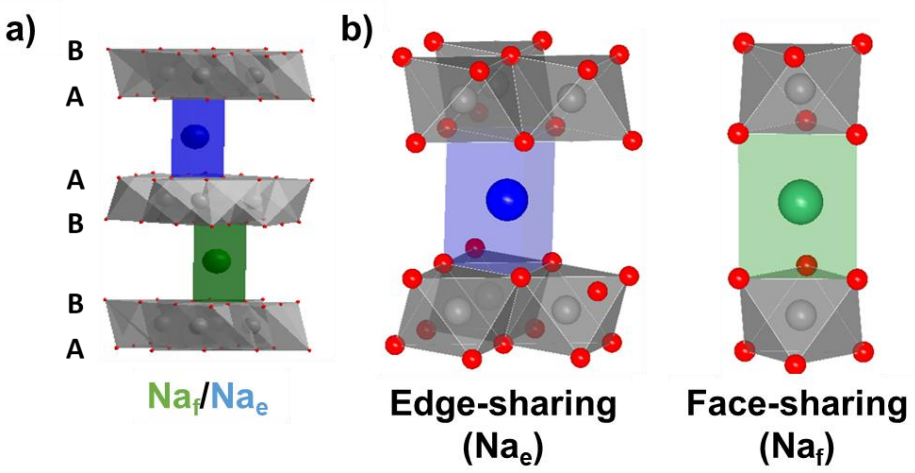

***Figure 1**: (a) Representation of the structure of layered P2-Na_xCoO_2. (b) local coordination environment of the Na_e (in blue) and Na_f (in green)*

The P2-Na_xCoO_2 layered phases were also investigated extensively in literature for their physical properties as thermoelectric and superconductivity performances (if hydrated)[12–18]. One interesting aspect in such layered cobalates is the co-existence of localized and itinerant electrons for some compositions. Foo *et al.*[19] reported the magnetic phases diagram of the P2-Na_xCoO_2 system and proposed a change of the magnetic regime from a "Curie-Weiss metal" regime for $x > 0.5$, with the co-existence of localized and itinerant electrons to a "Pauli metal" regime for $x < 0.5$ with only itinerant electrons. This was interpreted by strong electron correlations in the CoO_2 layers for $x > 0.5$, with on the triangular lattice, a fraction (1-x) of the sites occupied by itinerant spin-1/2 holes (Co^{4+}) hopping in a diamagnetic background of Co^{3+} ions[20]. In order to interpret those physical properties, Landron *et al.*[21] suggested that the trigonal distortion of CoO_6 octahedra along the c direction leads to the lift of degeneracy of the t_{2g} orbitals into two e_g' orbitals and one a_{1g} orbital as schematized on **Figure 2**. Therefore the band diagram considering this D_{3d} distortion has a narrow band at the Fermi level for a_{1g} and a broad brand for the e_g' levels providing respectively "heavy" charge carriers (localized electrons) and "light" charge carriers (delocalized electrons)[22].

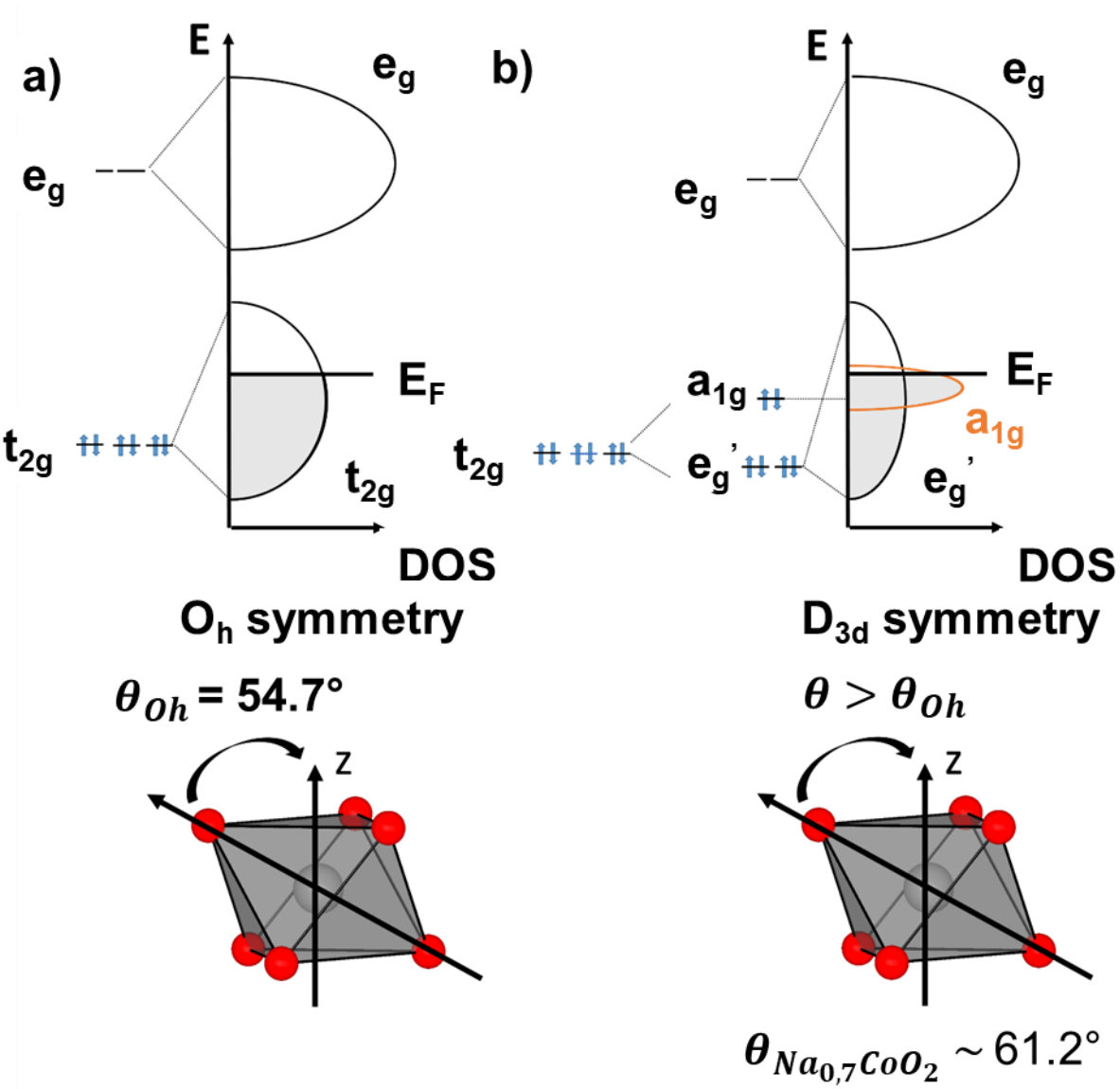

***Figure 2**: Schematic representation of the band structure of the Co ions in layered alkali cobaltates (a) without and (b) with considering the distortion of the CoO_6 octahedra perpendicularly to the CoO_2 layers. The θ angle represents the angle between the z axis parallel to the c_{hex} parameter and a Co-O bond direction. For a regular octahedral θ = 54.7°, whereas θ ~ 61.2° for P2-$Na_{\sim 0.7}CoO_2$.*

^{23}Na MAS NMR (Magic Angle Spinning Nuclear Magnetic Resonance) is a key tool to investigate both the local structure and electronic structure in such paramagnetic or metallic materials thank the hyperfine interactions (electron spin-nucleus spin coupling)[23]. In

paramagnetic compounds, as in the case of most of the positive electrode materials, the Fermi contact interactions mainly govern the signal position, according to:

$$\delta^{i}_{Fermi}(T) = \frac{1}{3SN_A}\rho^{i}(0)\chi_M(T) \qquad \text{eq(1)}$$

where S is the spin quantum number of the paramagnetic ion, $\rho^{i}(0)$ is the spin density on the *i* nucleus resulting from a spin transfer from the paramagnetic ions and χ_M the molar magnetic susceptibility (at the temperature of the NMR measurement). The spin transfer from the transition metal ion to the probed nucleus implies the local chemical bonds either by a delocalization (through orbital hybridization) or polarization mechanisms[24]. In metallic compounds, the spectra are dominated by Knight interactions leading to the following shift:

$$\delta_{Knight} = \frac{8\pi}{3}\langle|\psi_{r=0}|^2\rangle\chi^{e}_{s} \qquad \text{eq(2)}$$

where χ^{e}_{s} is the Pauli susceptibility of conduction bands electrons at Fermi level and $\langle|\psi_{r=0}|^2\rangle$ is the contribution of "s" orbitals at Fermi level of probed nucleus.

In recent studies[25,26], we used ^{7}Li and ^{23}Na solid state NMR to investigate the local structure, electronic structure and the dynamics in an original layered cobalt oxide: OP4-$Li_{0.42}Na_{0.38}CoO_2$, that exhibits Na and Li layers alternating along the c axis[27]. In particular, variable temperature ^{7}Li MAS NMR showed that NMR shifts result from two contributions: the Fermi contact and the Knight interaction due to the presence of both localized and delocalized electrons in the material[28,29].

In this paper, we aim to have a better insight of the mechanisms involved during cycling of P2-Na_xCoO_2 is used as positive electrode material in a Na cell. We thus studied the material evolution from the point of view of structure at different scales and of electronic properties upon charge up to high voltage (4.6 V) using a combination of ex-situ and operando XRD and ex situ

^{23}Na MAS NMR. Especially, the evolution of the NMR spectra (signal shape and shift) is discussed as a function of the local structure and electronic structure evolution. This study reveals a complex behavior due to the presence of localized and delocalized electrons in the electronic structure of the material resulting in a Fermi contact or Knight interactions respectively.

Experimental

Synthesis of the pristine phase

The synthesis of the pristine phase, P2-$Na_{0.7}CoO_2$, was performed using two precursors: Na_2CO_3 (Sigma Aldrich, 99.9 %, dried in an oven before the synthesis) and Co_3O_4 (home-made from cobalt nitrate and heat treated under air at 450 °C). Both precursors were mixed and ground in a glovebox filled with argon. Moreover, an excess of 5 % wt of Na_2CO_3 was added to the stoichiometric proportion because of the sodium high volatility at high temperature. The mixture was then heated in a furnace under O_2 at 900 °C for 12 h. The heating rate was set at 2 °C.min^{-1}. The product was then quenched to room temperature and entered directly in a Ar-filled glovebox. The XRD structural characterization of the pristine material can be found in **SI-1** for P2-$Na_{0.7}CoO_2$. **SI-2** shows the Scanning Electron Microscopy images obtained on the pristine phase.

Synthesis of the deintercalated phases

A floating technique was performed in order to synthetize the deintercalated phases with a precise control of the voltage to ensure the reproducibility of the results. These syntheses were performed in an airtight electrochemical cell using Na(s) / $NaPF_6$ in 1M Propylene Carbonate (PC) + 2% Fluoroethylene Carbonate (FEC) / P2-$Na_{0.7}CoO_2$ batteries**.** FEC was added to the electrolyte to limit its decomposition at high voltage[30]. The positive electrode, negative electrode

and the electrolyte were assembled in Swagelok type cells in an Ar-filled glovebox. The positive electrodes consist in a mixture of 90 mg of active material and 10 mg of black carbon with no binder. The mixture was pressed into pellets in the glovebox to form a dense positive electrode of about 100 mg. The electrochemical syntheses were realized in two steps as described on **Figure SI-3.** First**,** a galvanostatic step was performed at C/20 to the targeted voltage. Then, a potentiostatic step was used until the current reaches negligible values. The cell was then disconnected and entered in the glovebox where its voltage was measured before dissembling to be insured that the material is stable. Finally, the positive electrode powder was washed with DiMethyl Carbonate to remove any trace of electrolyte. *Ex-situ* XRD and ^{23}Na MAS NMR analyses were performed on the same Na_xCoO_2 sample.

Characterizations

ICP-OES

The chemical analysis of the Na and Co proportion of the pristine phase was realized by inductively coupled plasma-optical emission spectroscopy (ICP-OES) using a Varian Model 720-ES spectrometer. The powder was dissolved into a concentrated hydrochloric acid solution before analysis. The measured Na/Co ratio confirms the composition of $Na_{0.70(8)}CoO_2$ for the pristine phase.

Electrochemical measurements

The positive electrode was composed of P2-$Na_{0.70}CoO_2$ as active material mixed with Polytetrafluoroethylene (PTFE) as binder and a 50/50 wt mixture graphite/carbon black to improve the electronic conductivity in the electrode with a respective 88:2:10 mass ratio. The battery was assembled in a coin cell configuration in a dry Ar-filled glovebox. The galvanostatic

measurements were performed at 25 °C using a C/20 cycling rate between either 1.5 V and 4.3 V or between 1.5 V and 4.6 V.

XRD

The XRD characterization of the pristine sample was performed on a PANalytical X'Pert Pro diffractometer and equipped with Co $K_{\alpha_{1,2}}$ radiations. The sample was enclosed in the Ar glovebox in a hermetic aluminum sample holder with a Kapton window on the top. The measurements were performed between 5° and 135°. The profile refinement using the Rietveld method was realized with the software FullProf developed by J. Rodriguez-Carvajal[31] for 2θ from 15° to 85°.

The XRD analyses of the phases synthesized by electrochemistry were performed on a PANalytical X'Pert3 Powder diffractometer with a X'Celerator detector and equipped with Cu $K_{\alpha_{1,2}}$ radiations. The samples were enclosed in 0.3 mm-diameter glass capillaries sealed in the Ar glovebox. The measurements were performed between 10° and 80°. The profile refinements and structure refinements using the Rietveld method were realized with the FullProf software[32]. Due to the poor quality of the XRD acquisitions (Co fluorescence), we performed the Rietveld refinements of the XRD patterns by fixing the isotropic thermal factor (B_{iso} values) to 0.5 Å² for the Co and O ions and 1.0 Å² for the Na^+ ions. Moreover, the total Na^+ content was also fixed based on the electrochemical experiments. Therefore, we only refined the z position of the oxygen ions and the repartition of the occupancies between the two Na_e and Na_f sites.

In-situ Synchrotron XRD

High-angular resolution Synchrotron X-ray powder diffraction (SXRD) experiments were performed on the BL04-MSPD beamline of the ALBA Synchrotron[33] (Cerdanyola del Vallès,

Spain) on Na(s) / $NaPF_6$ in 1M Propylene Carbonate + 2% FEC / P2-$Na_{0.70}CoO_2$ cells and at room temperature. A $\lambda = 0.8261$ Å wavelength was used and data were recorded from $2\theta = 1.3°$ to $2\theta = 43.2°$. We used a specific home-made coin cell with 3 mm holes and pasted Kapton windows. Moreover, a thin aluminum foil between the Kapton window and the electrode was used as current collector on both sides of the coin cell. SXRD acquisitions were performed *operando* during the charge and the discharge of the battery at C/10 from 1.5 V to 4.6 V.

A succession of potentiostatic steps was performed from 4.1 V to 4.8 V with a step of 0.05 V and at a rate of C/10 in order to deeply charge the cell. The SXRD patterns were collected at the end of the different relaxations.

^{23}Na MAS NMR

The samples were introduced in a 2.5 mm zirconia rotors inside a glovebox. ^{23}Na MAS NMR was performed on a Bruker Avance spectrometer at 79.4 MHz (7 .05 T magnet). As the ^{23}Na nucleus is a quadrupolar nucleus with I = 3/2, a short pulse length of 1 µs corresponding to a $\pi/8$ pulse determined using an aqueous 1 M NaCl solution was employed. In these conditions, the main signal observed is due to the -1/2 → +1/2 central transition. The spectral width was set to 1 MHz, and the recycle time $D_0 = 0.2$ s, is long enough to avoid the *T1* saturation effects. The baseline distortions resulting from the spectrometer dead time (8 µs) were computationally removed using a polynomial baseline correction routine with the software DMFit[34].

Results and Discussion

Electrochemical cycling properties up to 4.6V vs Na^+/Na

Figure 3 shows the evolution of the voltage as a function of the theoretical Na^+ content (x) calculated from the electrode mass and applied current for a Na//P2-Na_xCoO_2 cell cycled at C/20 from 1.5 V to 4.3 V (**Figure 3a**) and 1.5V to 4.6V (**Figure 3b**). **Figure 3a** highlights the complexity of the P2-Na_xCoO_2 system with the presence of many voltage steps corresponding to the formation of phases with an ordering between filled and vacant Na^+ sites for specific sodium contents, in agreement with previous studies[7,11]. In the 1.5V-4.3V voltage range, all structural transitions are reversible and the cell exhibits a rather good capacity retention (**Figure SI-4**). When the cell is cycled up to 4.6 V, an additional voltage jump is clearly observed for x = 1/3 probably due to the presence of a peculiar ordered phase for this composition that will be discussed below. To our knowledge this phase has not been reported before, although its structure was predicted by DFT calculations[35,36]. The first discharge from 4.6 V (**Figure 3b**) looks much smoother without clear voltage drops compared to the first discharge curve from 4.3V and is located at lower voltage. Nevertheless, the voltage jumps reappear clearly during the following second charge indicating that the P2 structure is maintained. Then upon further cycling, all discharges do not exhibit any voltage steps whereas they are clearly observed upon charge. The origin of this behavior could be due to a strong difference in kinetics of the mechanisms occurring upon discharge compared to the ones involved upon charge. Although still unclear, this observation will be discussed a bit more below. When cycling between 1.5 and 4.6 V, a rapid capacity fading is also observed with only 78 % retention of the capacity after 40 cycles (**Figure SI-4).** Note that we indicated on **Figure 3** by dash lines**,** the selected voltages used to prepare the different P2-Na_xCoO_2 phases used for the *ex-situ* ^{23}Na MAS NMR and XRD studies performed on the same samples as described in the experimental section.

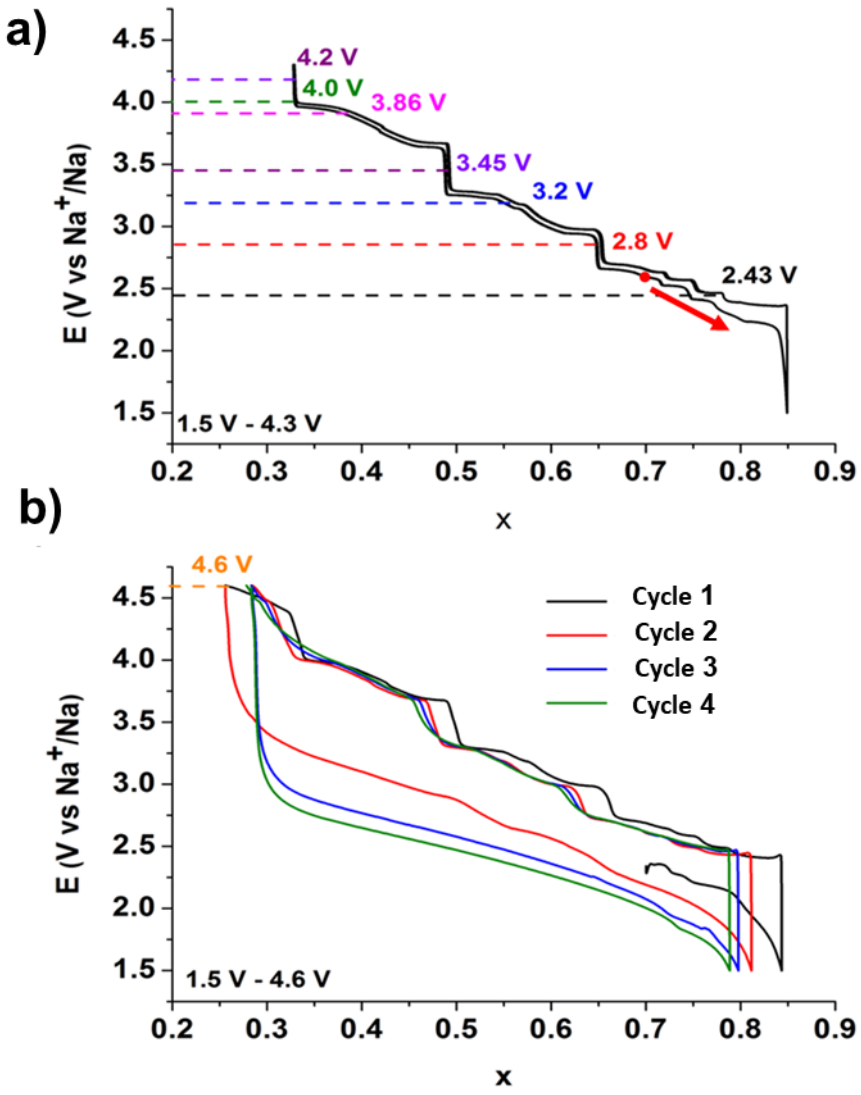

***Figure 3**: a) Two first galvanostatic cycles at C/20 of Na(s)//P2-Na_xCoO_2 batteries in the 1.5-4.3 V range The colored dashed lines correspond to the voltage applied to synthetize the different Na_xCoO_2 phases studied by ex-situ XRD and NMR. b) Four first galvanostatic cycles at C/20 of Na(s)//P2-Na_xCoO_2 batteries in the 1.5 V-4.6 V range.*

Evolution of the average structure upon cycling

In addition to our previous work carried out by *in-situ* XRD[11], we could investigate the evolution of the average structure of P2-Na_xCoO_2 system up to higher voltage, thanks to the use of FEC additive in the electrolyte and the use of Synchrotron radiation. A Na(s)// P2-$Na_{0.70}CoO_2$ cell was initially discharged to 1.5V and the *operando* SXRD study was performed during the full first

charge from 1.5 V to 4.6 V using a C/10 cycling rate. The collected patterns are displayed in **Figure 4**. Some additional peaks on the different patterns are due to the different elements in the cell as carbon graphite, PTFE, Al and Na foil.

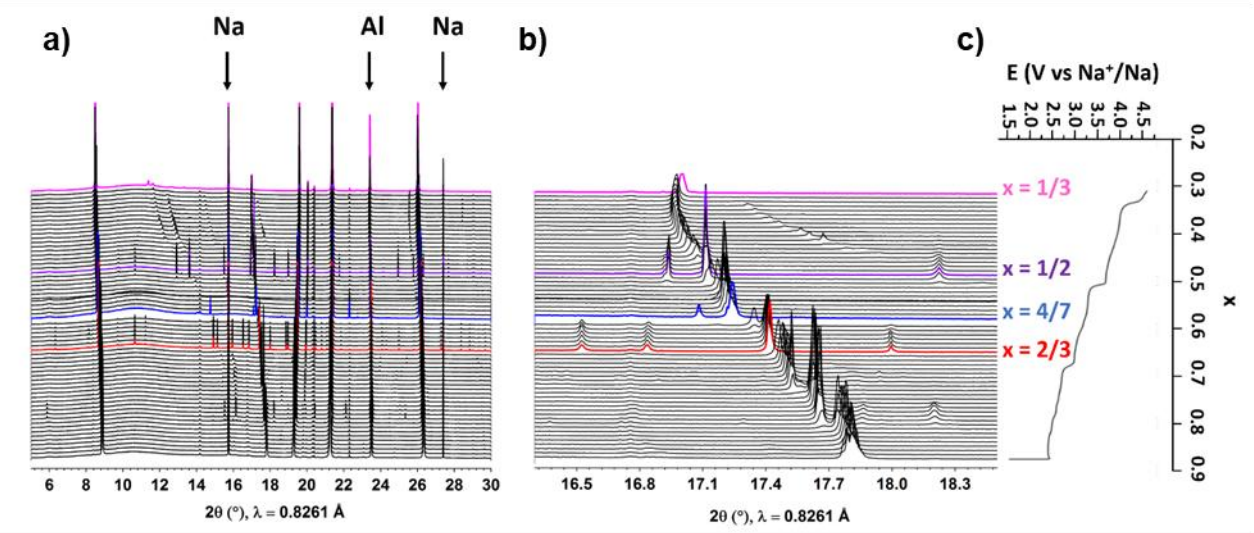

***Figure 4 (two columns)**: a) XRD patterns obtained by operando SXRD on the P2-Na_xCoO_2 system on the first charge from 1.5 V to 4.6 V at C/10 in the 5 – 30° range. The colored lines represent the XRD patterns of the peculiar phases $Na_{2/3}CoO_2$, $Na_{4/7}CoO_2$, $Na_{1/2}CoO_2$ and $Na_{1/3}CoO_2$. b) Zoom in the 16.3 - 18.5° range. c) Corresponding galvanostatic cycling at C/10 of the Na(s)//P2-Na_xCoO_2 battery.*

Up to 3.8 V vs Na^+/Na, the structural evolution is in agreement with our previous results[11]: i) the c_{hex} lattice parameter increases as the Na^+ content decreases as seen by the shift of the (004) line toward lower angles (**Figure 4b**), ii) peculiar significant number of various phases is observed in the $0.5 \leq x \leq 0.9$ range with an alternation of biphasic and solid solution domains as well as peculiar ordered phases iii) in particular the ordered $Na_{2/3}CoO_2$, $Na_{4/7}CoO_2$, $Na_{1/2}CoO_2$ phases are clearly identified as seen from the well identified superstructure peaks. The corresponding patterns have been refined with the Le Bail technique in agreement with structural models previously reported (**SI-5**)[11,18,37,38]. For 3.8 V < V < 4.6 V, the P2 structure is still maintained, and

the (004) peak position is almost constant, suggesting that the structure has reached a maximal c_{hex} lattice parameter value (~11.20 Å) despite further Na^+ ions deintercalation. Moreover, a new diffraction line appears for x < 0.4 at 17.7° and its position shifts toward low angles when the voltage increases indicating a pseudo-solid solution domain probably due to the presence of incommensurate structures. In the XRD pattern recorded at 4.6 V (last pattern), those peaks have disappeared and new diffraction lines are observed in the 11-14° region indicating a new superstructure that corresponds to the x = 1/3 composition, as shown in **Figure SI-6**. We proposed a $\sqrt{3}$a x $\sqrt{3}$a x 3c superlattice to refine this XRD patterns. The corresponding space group is $P6_1$ with a = b = 4.867(1) Å and c = 33.613(1) Å. Unfortunately, we could not propose a $Na^+/\square$ ordering model within this supercell to further proceed with a full Rietveld refinement. Note that the (004) peak intensity slightly decreases which could be the sign of the P2 structure instability and the beginning of sheets glidings as often observed in layered materials[39,40]. In order to further investigate the phases structural modifications at high voltage, another cell was studied by *in-situ* SXRD, charged up to 4.1V at C/10 followed by a succession of potentiostatic steps between 4.1 and 4.8 V. SXRD patterns were collected at the end of the relaxation period when the material reached an equilibrium state (**Figure 5 and Figure SI-7**). In agreement with the operando study, from 4.1 V to 4.55 V, the average structure remains P2. At 4.6 V, the P2 structure is still maintained but the (002) line starts to broaden and appears with some asymmetry toward higher 2Θ angle that is usually due to the formation of stacking faults (**Figure 5a**). One can expect some "O"-type stacking faults in this structure (**Figure SI-8**). From 4.65 to 4.8 V, the (00l) diffraction lines strongly broaden and shift to larger angle values characteristic of a decrease of the c_{hex} lattice parameter. In addition, the (h0l) diffraction lines broaden and become asymmetric. The peaks asymmetry and the decrease of the c_{hex} lattice parameter confirm the

presence of sheets glidings leading to a strong disorder in the material. The sheets glidings were already reported by Komaba and coworkers[38] and more recently by Billaud *et al.*[39] on other P2-systems by *ex-situ* XRD. Note that in these papers, the phases were determined in an OP4 structure considering that the Na^+ ions are intercalated in prismatic and octahedral sites after the P2-OP4 phase transition. In our study, the phase obtained at high voltage is called "OP" phase and not OP4 due to the absence of a long range ordering along the c axis contrary to the OP4-(Na,Li)CoO_2 phase studied by some of us[26,27,25]. Note also that in a previous publication of our group, this disordered "OP" phase was called "Z" phase in the P2-$Na_xMn_{1/2}Fe_{1/2}O_2$ system[41]. The formation of this disordered phase starts to appear at 4.6V and be, at least, partially the origin of the large polarization observed upon discharge. If the "O" defects appears first at the surface of the particles, Li^+ intercalation kinetics may be slow down versus intercalation in the "P" type interslab.

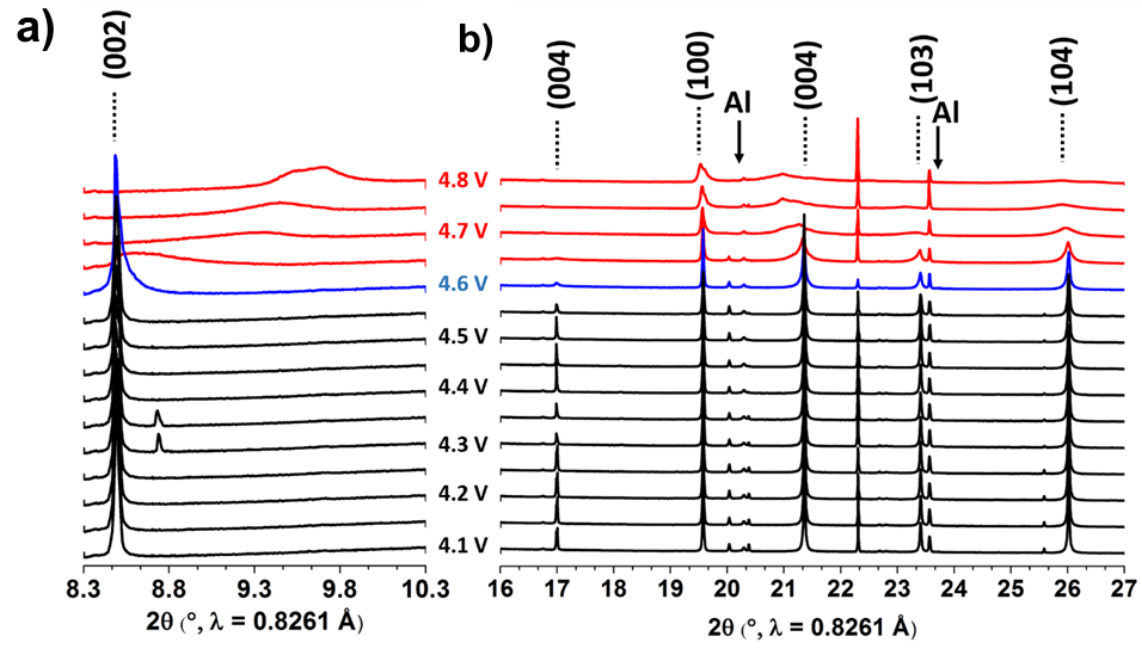

***Figure 5 (two columns)**: a) XRD patterns of stabilized P2-Na_xCoO_2 phases by potentiostatic steps at different voltages from 4.1 V to 4.8 V for 8.3 < 2θ < 10.3° b) for 16 < 2θ < 27°.*

In order to study the phases at a local scale, we used *ex-situ* XRD. Some P2-Na_xCoO_2 phases were thus prepared at different voltages, as indicated on **Figure 3**. After washing, each electrode has been split in two part in order perform XRD and NMR experiments on a same sample. All XRD patterns (**Figure SI-9)** could be refined using the Rietveld method in the *$P6_3/mmc$* space group of the P2 stacking, except the pattern of the phase recovered after the potentiostatic step at 4.6V, that exhibit an "OP" disordered phase. An example of Rietveld refinement is shown on **Figure SI-10** for P2-$Na_{0.40}CoO_2$. **Figure 6** gives the evolution of the c lattice parameter versus the Na^+ content resulting from both *in-situ* and *ex-situ* studies showing a very good agreement. **Figure 7a** gives the evolution of the O-Na-O interslab and CoO_2 slab thicknesses. The O-Na-O interslab thickness increases during charge to a maximal value around x ~ 0.4, while the CoO_2 slabs thickness slightly decreases. The increase of the O-Na-O layers thickness is in agreement with the Na^+ deintercalation and the increase of the O-O repulsions between the layers. The decrease of the CoO_2 slabs thickness is coherent with the oxidation of Co^{3+} to Co^{4+}, which increases the Co-O covalency. The "OP" phase recovered at 4.6V exhibits a lower average O-Na-O layers thickness due to "O"-type layer formation leading to a c parameter value (considering a two layer stacking) equal to 10.05 Å. This evolution in slab and interslab thickness will be used in the following to discuss the evolution of the ^{23}Na NMR shifts. **On Figure 7b and 7c** the mean bonds distances in the NaO_6 prisms and CoO_6 octahedra are indicated for two selected compounds: P2-$Na_{0.33}CoO_2$ and P2-$Na_{0.67}CoO_2$. The evolution of the Na sites occupation versus x is shown on **Table SI-11**. In the pristine material, around 2/3 of Na^+ ions are located in the Na_e sites (sharing edges with CoO_6 octahedra) and 1/3 in the Na_f one (sharing faces with CoO_6 octahedra). As x decreases, the amount of Na^+ ions in the Na_f sites remains rather constant while the amount of Na^+ ions in the Na_e sites largely decreases until reaching the x = 0.5 composition

with half occupation of both sites. For lower Na content ($1/3 < x < 0.5$), the Na^+ ions in Na_f sites mainly decreases. For $x = 1/3$, the Na^+ ions occupy almost only the Na_e sites.

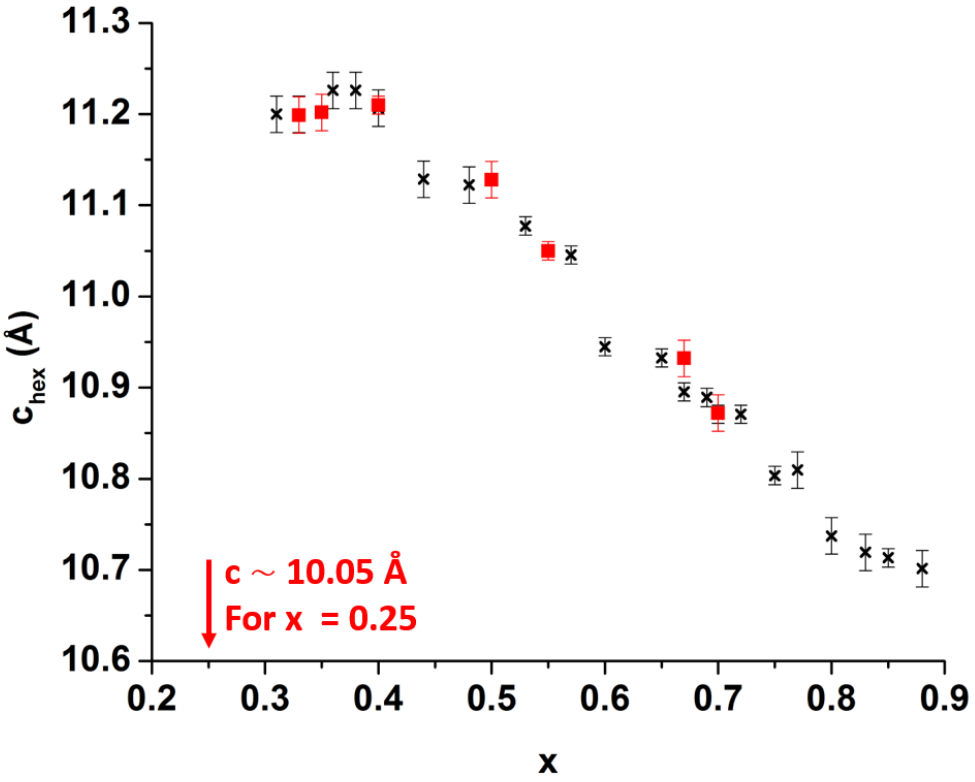

***Figure 6**: Evolution of c_{hex} lattice parameter as a function of x. The black crosses represent the lattice parameters extracted from the SXRD patterns and the red squares are the values calculated with Rietveld refinements from the ex-situ laboratory XRD patterns*

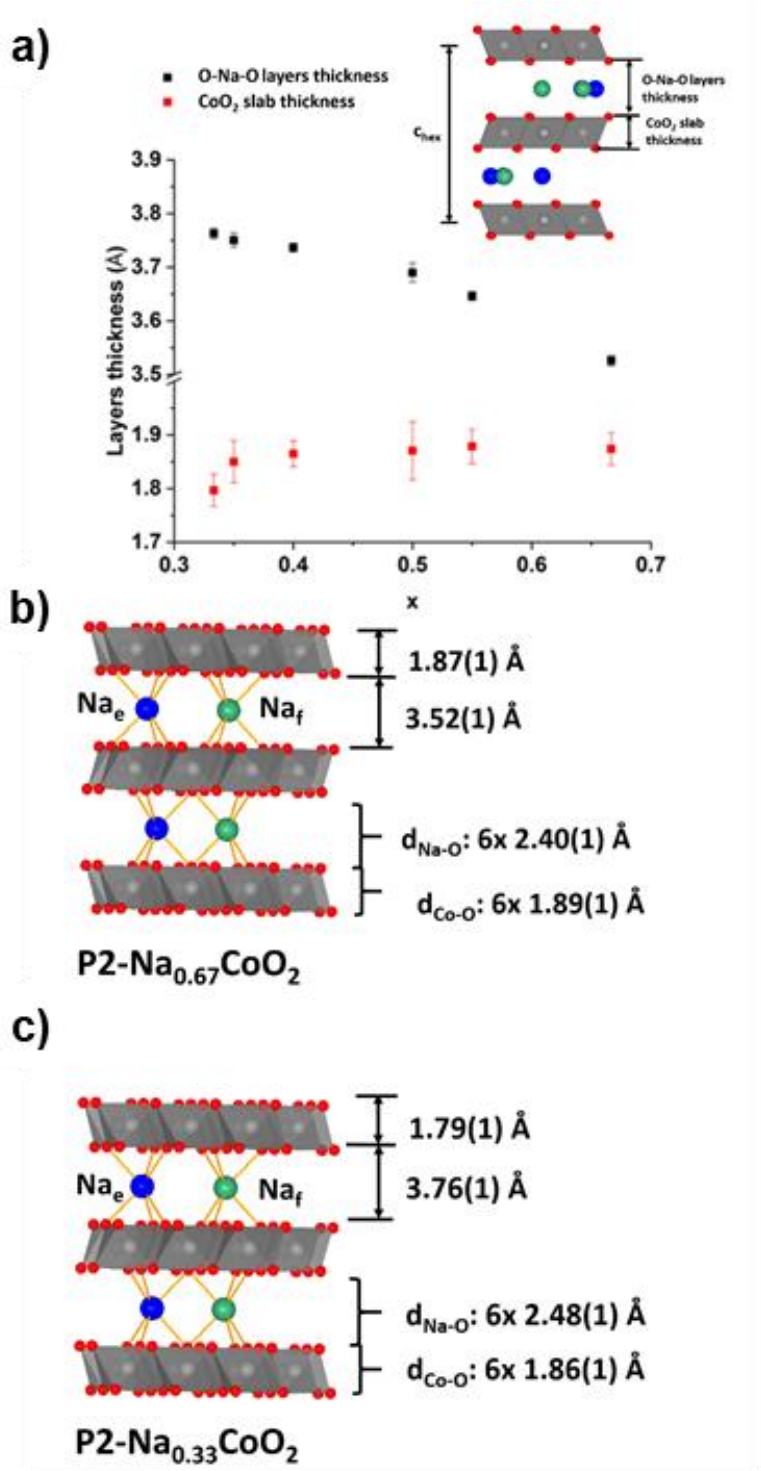

***Figure 7**: a) Evolution of the O-Na-O layers and CoO_2 slab thickness for P2-Na_xCoO_2 (insert: schematic representation of the P2-stacking). Comparison of the different distances in b) P2-$Na_{0.67}CoO_2$ and c) P2-$Na_{0.33}CoO_2$*

Evolution of the local structure and electronic structure upon cycling

Figure 8 represents the ^{23}Na MAS NMR spectra recorded for the P2-Na_xCoO_2 compounds. In the $0.33 \leq x \leq 0.82$ composition range, a single signal with a typical 2nd order interaction lineshape is observed. Due to strong Na^+ ion mobility in the interslab space versus the NMR timescale, an average signal between the two Na_e and Na_f sites is observed[42]. The spectra were fitted using the DMFit software[34] and the parameters are reported in **Table SI-12**. It appears that the quadrupolar interaction decreases as the sodium content decreases and the isotropic shifts varies in different manner depending of the Na content as discussed in the following. The evolution of the mean quadrupolar constant might be due to several factors occurring upon Na^+ deintercalation associated to Co ions oxidation: evolution of the local geometry around Na^+ ions, evolution of the hopping rate between Na_e and Na_f and relative site occupancy and evolution of the Co-O covalency and partial charges.

Considering the large values obtained for the isotropic shifts, we consider that they result mainly from two contributions: the Fermi contact and the Knight interaction due to the presence of, respectively, localized and delocalized electrons. The Fermi contact shift depends on the magnitude of the electronic spin transferred from the transition metal ions to the probed nucleus through the chemical bonds (eq (1)). This interaction, therefore, strongly depends on the number of unpaired localized electrons of Co^{n+} ions, on their 3d-type orbital occupancy and on the local hybridization between the Co 3d, O 2p and Na 3s orbitals. It is therefore very sensitive to both the local structure and electronic structure. The Knight shift depends on the contribution of the Na 3s orbital at the Fermi level where the delocalized electrons are involved.

Thus, here we can expressed the total isotropic shift by:

$$\delta_{total} = \delta_{Fermi} + \delta_{Knight}$$

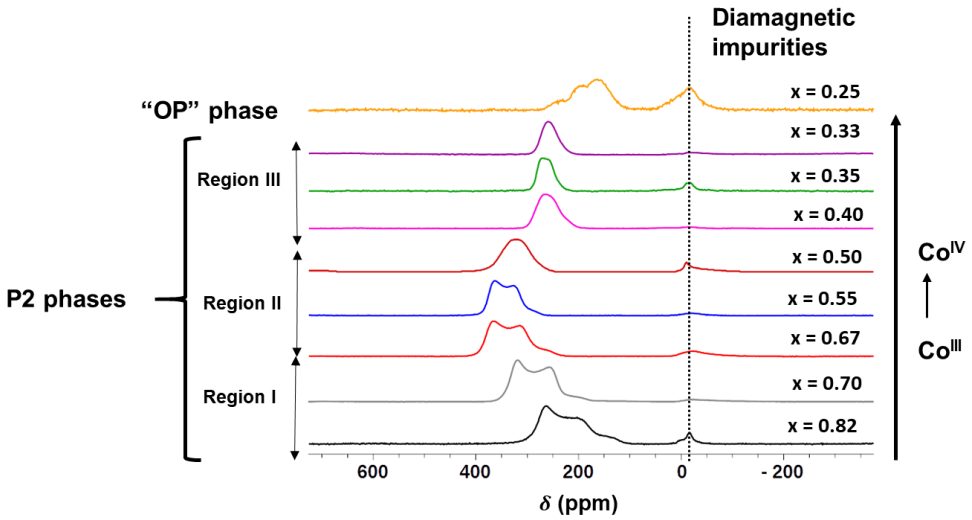

***Figure 8**: Evolution of ^{23}Na MAS NMR signals of the P2-Na_xCoO_2 phases using a 7.05 T magnetic field (ν_R = 30 kHz) and single pulse sequences. The signals intensities are arbitrary chosen to better visualize the shifts and the shape evolution.*

In order to interpret the NMR shift evolution and to make the link with the mechanisms involved during the Na^+ deintercalation, we need to consider several main factors: the local geometric evolution, the local electronic structure evolution and the transition from a "Curie-Weiss metal" regime to a "Pauli metal" regime occurring at x = 0.5[15]. For the first aspect, the mean Na-O distances increases as x decreases mainly due to the c-axis expansion up to x = 0.40 as already mentioned (**Figure 7a**), simultaneously the CoO_6 octahedra are compressed and exhibit shorter Co-O distances due to the increase of the Co-O bond covalency. Overall, we expect from this factor a lower efficiency of the Co^{n+}-O-Na spin transfer mechanism from Co to Na nucleus as x decreases if the Co^{n+} mean charge is maintained constant and thus a decrease of the Fermi contact shift. Additionally, the local electronic structure evolves as x decreases considering the oxidation of diamagnetic LS-Co^{3+} ($t_{2g}^6e_g^0$) into paramagnetic LS-Co^{4+} ($t_{2g}^5e_g^0$): the more paramagnetic is the mean Co^{n+} ion, the larger will be the Co^{n+}-O-Na spin transfer mechanism given local

geometry, i.e, if the Co-O-Na distances and angles are maintained constant and thus an increase of the Fermi contact shift. Finally, the "Curie-Weiss metal" regime to a "Pauli metal" regime transition occurs at $x = 0.5$[15] due to the different relative a_{1g} and e'_g orbitals occupancy and/or less localization effect of the charge on Co ions induced by adjacent Na^+ layers**.** An evolution from a Fermi contact shift to a Knight shift is therefore expected.

Those factors are sometimes antagonist regarding their effect on the ^{23}Na MAS NMR isotropic signal position evolution depending of Na^+ content (x). For more clarity, we will discuss below the evolution observed versus the Na content in three composition regions as indicated in **Figure 8 and 9**.

In **Region I** ($0.67 \leq x \leq 0.82$), the NMR shift increases as x decreases. The main contribution of shift here is clearly the Fermi contact interaction that becomes stronger as the number of paramagnetic Co^{4+} ions increases, despite the weaker Co^{n+}-O-Na orbital overlap. Therefore, a majority of the electrons have a localized behavior in agreement with the increase of the molar magnetic susceptibility $\chi(T)$ observed for $0.64 \leq x \leq 0.7$ by Igarashi *et al*[43]. It is reasonable to believe then that new holes are mainly formed in the a_{1g} band of the electronic structure (**Figure 2**). In **Region II** ($0.5 \leq x \leq 0.67$), the NMR shift significantly decreases when x decreases despite the further oxidation of the Co^{3+} (diamagnetic) ions to Co^{4+} ions (paramagnetic). Although, those samples are still in the "Curie-Weiss metal" as reported by Foo *et al*.[19], a moderate increase of $\chi(T)$ was observed for $0.52 \leq x \leq 0.58$[42] with absolute value rather close to Pauli paramagnetic state. Since the observed shift is not constant, but decreases for $0.5 \leq x \leq 0.67$, we believe that the evolution of the local geometry is the predominating effect here. The increase of the interslab space results in a weaker 3d Co^{n+}- 2p O- 3s Na orbital overlap and thus to a weaker electronic spin transfer to Na nuclei that is also associated to a progressive change in

the localization of new holes from the a_{1g} to the e_g' band. In **Region III** ($0.33 \leq x \leq 0.5$), an important decrease of the NMR shifts, compared to the values in the **Region II** is observed. This can be interpreted by the change of physical properties of the P2-Na_xCoO_2 phase from "Weiss metal" to "Pauli metal" that exhibits only delocalized electrons. The shift here is then mainly governed by the Knight interaction (the Na 3s orbital participation to the Knight shift seems to be almost constant during the Na^+ deintercalation). It is reasonable to believe then that new holes are mainly formed in the e_g' band.

Finally, the ^{23}Na MAS NMR signal of the phase prepared at high voltage (V = 4.6 V, x = 0.25) is largely broadened and three contributions can be observed**.** The presence of these new Na^+ environments is assigned to the formation of the "OP" disordered phase due to slabs glidings and agrees with the observation reported by Clément *et al.*[44] for Na_xMnO_2 with $x \sim 0.2$. Na^+ ions might be located in O-type or P-type interslab space.

In order to discuss the reversibility of the sodium deintercalation process, when the battery is cycled up to 4.6 V, XRD patterns and NMR spectra have been also recorded on materials recovered at 2.4 V vs Na^+/Na after a charge at 4.3 V or at 4.6 V (**Figure SI-13**). No significant changes at the mean and local structure is observed despite a real difference in the electrochemical discharge curves (**Figure 3**), showing that the material did not undergo severe structure damage while the battery reached 4.6 V. Nevertheless, a much larger signal intensity is observed in the 0 ppm region indicating the formation of a diamagnetic phase, probably amorphous as not seen by XRD, that would result from a thick cathode electrolyte interphase (CEI) formation. This indicates that the high polarization observed during the first discharge while charging up to 4.6 V is mainly due to kinetics effects as discussed earlier since the electrochemical study shows a good reversibility at the second discharge. This kinetics limitation

can either be due to the thick CEI that might be unstable and involved in a dynamic evolution of dissolution-deposition over charge-discharge cycles as reported for some layered oxides[45] and/or to the formation of the "OP" phase predominantly at the surface of the particles that would lead to a lower kinetics of Na^+ reintercalation or "asymmetric" (more Na+ reintercalated in the "P"-type layers before the sheets are gliding back to P2).

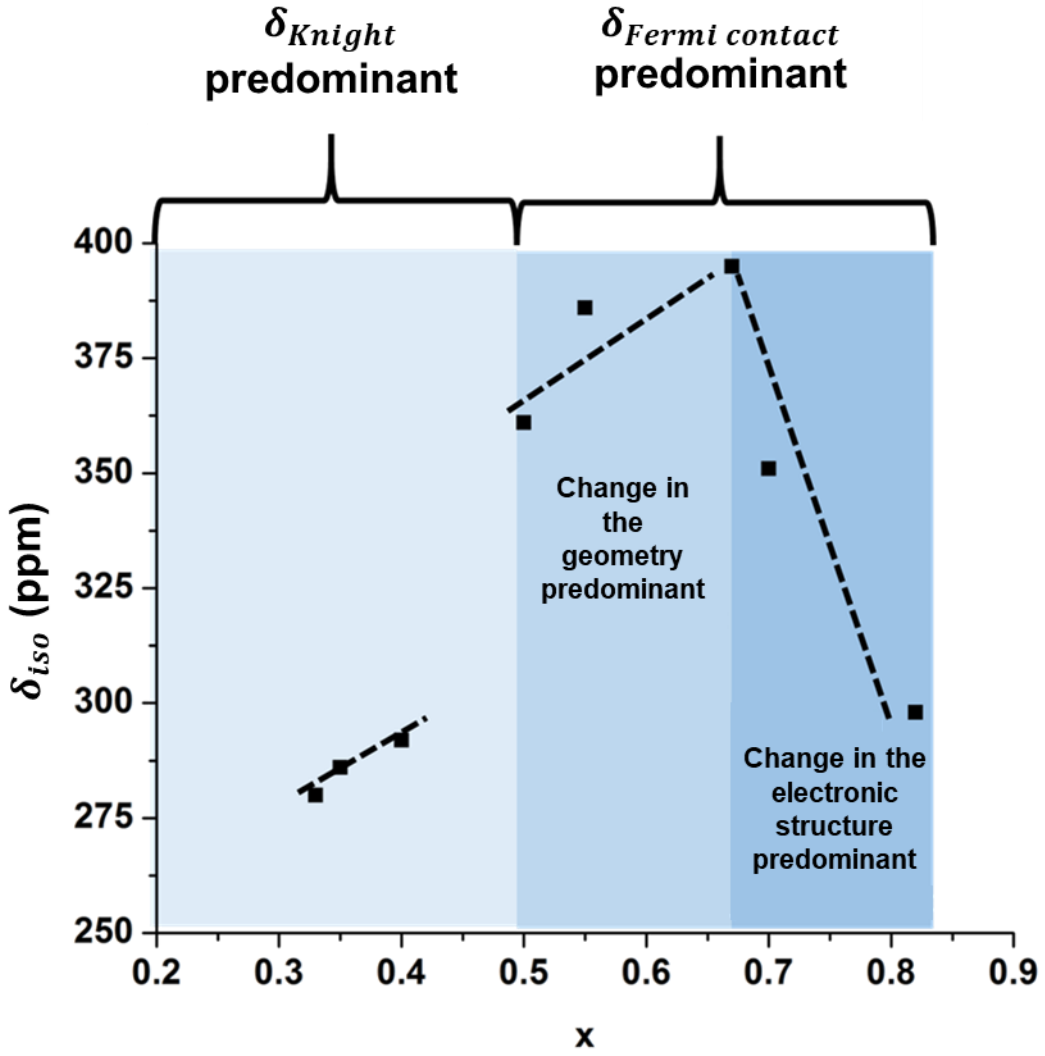

Figure 9. *Shift evolution and description of the phenomena responsible ^{23}Na MAS NMR isotropic as a function of the Na^+ content*

Conclusion

Using Synchrotron XRD, we studied the P2-Na_xCoO_2 phase diagram upon charge with a specific attention to the structural modifications occurring at high voltage: the presence of an ordered phase for x = 1/3 is observed above 4.3 V vs Na^+/Na, the P2 stacking becomes unstable and slab glidings occur to form a disordered structure with a stacking of O-type and P-type interslab space. ^{23}Na MAS NMR has been used to investigate the local structure and electronic property evolution upon charge. This study reveals a complex behavior due to the presence of localized and delocalized electrons in the material resulting in a Fermi contact interaction and Knight interaction, respectively, that co-exist here with relative amount depending on the Na content. The ^{23}Na NMR shift evolution versus Na content was interpreted by considering the predominant influence of structural factors (linked to the strength of Co-O-Na orbital overlap and thus to the efficiency of spin transfer mechanism) or electronic (such as the formal quantity of paramagnetic Co^{4+} ions, and the relative amount of localized and delocalized electrons).

Unfortunately Density Functional Theory (DFT) calculations to support the discussion of the shift evolution as we have done previously[24,46–48] could not be used here. Indeed, modelling "Curie-Weiss metal" can be satisfactory done using DFT. For example, neither Generalized Gradient Approximation (GGA) nor GGA+U allow a correct description of the electronic structure of such layered cobalt oxides that exhibits localized and delocalized electrons. In GGA, the inherent self-interaction error has a detrimental effect on localized transition-metal d orbitals and the addition of a Hubbard U correction has been shown to yield some unphysical results for layered cobalt oxide systems as incorrect phase diagram for the P2-Na_xCoO_2 system[49].

Finally, we could interpret the large polarization observed upon discharge while cycling up to 4.6V by a kinetic limitation that can either be due to the formation of a thick CEI at high voltage, probably unstable upon discharge and/or to the formation of the "OP" phase predominantly at the surface.

ASSOCIATED CONTENT

Supporting Information

Experimental and refined XRD patterns and SEM images of the pristine material; Principle of the electrochemical preparation of the Na_xCoO_2 compounds studied; Evolution of the specific capacity in the 1.5 – 4.3 V range and in the 1.5 – 4.6 V range at C/20; XRD refinement results on P2-Na_xCoO_2 peculiar phases with Na+/vacancy ordering; In situ Potentiostatic measurements on P2-Na_xCoO_2 as a function of time and corresponding XRD patterns; Representation of the CoO_2 stacking in an ideal P2 structure and in a P2 structure with an O-type stacking fault after sheets glidings ; Ex-situ capillary laboratory XRD patterns of the Na_xCoO_2 phases studied by ^{23}Na MAS NMR and corresponding structural parameters after Rietveld refinements; fitted ^{23}Na NMR parameters; XRD patterns ^{23}Na MAS NMR spectra of the pristine P2-phase and two P2-Na_xCoO_2 phases recovered at 2.4 V after a charge at 4.3 and 4.6 V (vs Na^+/Na).

AUTHOR INFORMATION

Corresponding Author

Dany Carlier – Univ. Bordeaux, CNRS, Bordeaux INP, ICMCB, UMR 5026, F-33600 Pessac, France; orcid.org/0000-0002-5086-4363

Authors

Yohan Biecher – Univ. Bordeaux, CNRS, Bordeaux INP, ICMCB, UMR 5026, F-33600 Pessac, France ; https://orcid.org/0000-0001-8486-3505
Anthony Baux – Univ. Bordeaux, CNRS, Bordeaux INP, ICMCB, UMR 5026, F-33600 Pessac, France
Francois Fauth - CELLS - ALBA synchrotron, Cerdanyola del Vallès, E-08290 Barcelona, Spain; https://orcid.org/0000-0001-9465-3106
Claude Delmas – Univ. Bordeaux, CNRS, Bordeaux INP, ICMCB, UMR 5026, F-33600 Pessac ; https://orcid.org/0000-0002-8188-0067
Gillian R. Goward - Department of Chemistry & Chemical Biology, McMaster University, Hamilton, Ontario L8S 4M1, Canada; https://orcid.org/0000-0002-7489-3329

Acknowledgments

This work beneficiates from financial support from the Fond Franco-Canadien pour la Recherche (FFCR). ALBA synchrotron is acknowledged for granting beamtime through proposal no 2017092426. We are also grateful to Mathieu Duttine for its technical support.

References

(1) Fouassier, C.; Matejka, G.; Reau, J.-M.; Hagenmuller, P. Sur de Nouveaux Bronzes Oxygénés de Formule Na_xCoO_2 (X < 1). Le Systeme Cobalt-Oxygene-Sodium. *J. Solid State Chem.* **1973**, *6* (4), 532–537.
(2) Mizushima, K.; Jones, P. C.; Wiseman, P. J.; Goodenough, J. B. Li_xCoO_2 (0< x<1): A New Cathode Material for Batteries of High Energy Density. *Mater. Res. Bull.* **1980**, *15* (6), 783–789.
(3) Braconnier, J.-J.; Delmas, C.; Fouassier, C.; Hagenmuller, P. Comportement Electrochimique Des Phases Na_xCoO_2. *Mater. Res. Bull.* **1980**, *15* (12), 1797–1804.
(4) Delmas, C.; Braconnier, J.-J.; Fouassier, C.; Hagenmuller, P. Electrochemical Intercalation of Sodium in Na_xCoO_2 Bronzes. *Solid State Ion.* **1981**, *3*, 165–169.
(5) Nitta, N.; Wu, F.; Lee, J. T.; Yushin, G. Li-Ion Battery Materials: Present and Future. *Mater. Today* **2015**, *18* (5), 252–264. https://doi.org/10.1016/j.mattod.2014.10.040.
(6) Delmas, C. Sodium and Sodium-Ion Batteries: 50 Years of Research. *Adv. Energy Mater.* **2018**, *8* (17), 1703137. https://doi.org/10.1002/aenm.201703137.
(7) Lei, Y.; Li, X.; Liu, L.; Ceder, G. Synthesis and Stoichiometry of Different Layered Sodium Cobalt Oxides. *Chem. Mater.* **2014**, *26* (18), 5288–5296. https://doi.org/10.1021/cm5021788.
(8) Baskar, S.; Sada, K.; Barpanda, P. Layered P2-Na_xCoO_2 and Na_xFeO_2 as Cathode Materials for Potassium-Ion Batteries. *ECS Trans.* **2017**, *80* (10), 357–364. https://doi.org/10.1149/08010.0357ecst.
(9) Yoncheva, M.; Stoyanova, R.; Zhecheva, E.; Kuzmanova, E.; Sendova-Vassileva, M.; Nihtianova, D.; Carlier, D.; Guignard, M.; Delmas, C. Structure and Reversible Lithium Intercalation in a New P'3-Phase: $Na_{2/3}Mn_{1-y}Fe_yO_2$ (Y = 0, 1/3, 2/3). *J. Mater. Chem.* **2012**, *22* (44), 23418. https://doi.org/10.1039/c2jm35203f.
(10) Delmas, C.; Fouassier, C.; Hagenmuller, P. Structural Classification and Properties of the Layered Oxides. *Phys. BC* **1980**, *99* (1–4), 81–85. https://doi.org/10.1016/0378-4363(80)90214-4.

(11) Berthelot, R.; Carlier, D.; Delmas, C. Electrochemical Investigation of the P2–Na_xCoO_2 Phase Diagram. *Nat. Mater.* **2011**, *10* (1), 74–80. https://doi.org/10.1038/nmat2920.
(12) Terasaki, I.; Sasago, Y.; Uchinokura, K. Large Thermoelectric Power in $NaCo_2O_4$ Single Crystals. *Phys. Rev. B* **1997**, *56* (20), R12685–R12687. https://doi.org/10.1103/PhysRevB.56.R12685.
(13) Takada, K.; Sakurai, H.; Takayama-Muromachi, E.; Izumi, F.; Dilanian, R. A.; Sasaki, T. Superconductivity in Two-Dimensional CoO_2 Layers. *Nature* **2003**, *422* (6927), 53–55. https://doi.org/10.1038/nature01450.
(14) Chou, F. C.; Cho, J. H.; Lee, P. A.; Abel, E. T.; Matan, K.; Lee, Y. S. Thermodynamic and Transport Measurements of Superconducting $Na_{0.3}CoO_2{\cdot}1.3H_2O$ Single Crystals Prepared by Electrochemical Deintercalation. *Phys. Rev. Lett.* **2004**, *92* (15), 157004. https://doi.org/10.1103/PhysRevLett.92.157004.
(15) Landron, S.; Lepetit, M.-B. Ab Initio Evaluation of the Local Effective Interactions in the Superconducting Compound $Na_{0.35}CoO_2 \cdot 1.3\ H_2O$. *Phys. Rev. B* **2006**, *74* (18), 184507. https://doi.org/10.1103/PhysRevB.74.184507.
(16) Lee, M.; Viciu, L.; Li, L.; Wang, Y.; Foo, M. L.; Watauchi, S.; Pascal Jr, R. A.; Cava, R. J.; Ong, N. P. Large Enhancement of the Thermopower in Na_xCoO_2 at High Na Doping. *Nat. Mater.* **2006**, *5* (7), 537–540. https://doi.org/10.1038/nmat1669.
(17) Lee, M.; Viciu, L.; Li, L.; Wang, Y.; Foo, M. L.; Watauchi, S.; Pascal, R. A.; Cava, R. J.; Ong, N. P. Enhancement of the Thermopower in in the Large-X Regime (0 > 0.75). *Phys. B Condens. Matter* **2008**, *403* (5–9), 1564–1568. https://doi.org/10.1016/j.physb.2007.10.320.
(18) Huang, Q.; Foo, M. L.; Lynn, J. W.; Zandbergen, H. W.; Lawes, G.; Wang, Y.; Toby, B. H.; Ramirez, A. P.; Ong, N. P.; Cava, R. J. Low Temperature Phase Transitions and Crystal Structure of $Na_{0.5}CoO_2$. *J. Phys. Condens. Matter* **2004**, *16* (32), 5803–5814. https://doi.org/10.1088/0953-8984/16/32/016.
(19) Foo, M. L.; Wang, Y.; Watauchi, S.; Zandbergen, H. W.; He, T.; Cava, R. J.; Ong, N. P. Charge Ordering, Commensurability, and Metallicity in the Phase Diagram of the Layered Na_xCoO_2. *Phys. Rev. Lett.* **2004**, *92*, 247001. https://doi.org/10.1103/PhysRevLett.92.247001.
(20) Wang, Y.; Rogado, N. S.; Cava, R. J.; Ong, N. P. Spin Entropy as the Likely Source of Enhanced Thermopower in $Na_xCo_2O_4$. *Nature* **2003**, *423* (6938), 425–428. https://doi.org/10.1038/nature01639.
(21) Landron, S.; Lepetit, M.-B. Importance of t_{2g}-E_g Hybridization in Transition Metal Oxides. *Phys. Rev. B* **2008**, *77* (12), 125106.
(22) Singh, D. J. Electronic Structure of $NaCo_2O_4$. *Phys. Rev. B* **2000**, *61* (20), 13397.
(23) Gotoh, K. ^{23} Na Solid-State NMR Analyses for Na-Ion Batteries and Materials. *Batter. Supercaps* **2021**, batt.202000295. https://doi.org/10.1002/batt.202000295.
(24) Carlier, D.; Ménétrier, M.; Grey, C. P.; Delmas, C.; Ceder, G. Understanding the NMR Shifts in Paramagnetic Transition Metal Oxides Using Density Functional Theory Calculations. *Phys. Rev. B* **2003**, *67,* 174103. https://doi.org/10.1103/PhysRevB.67.174103.
(25) Berthelot, R.; Pollet, M.; Carlier, D.; Delmas, C. Reinvestigation of the OP4-(Li/Na)CoO_2-Layered System and First Evidence of the (Li/Na/Na)CoO_2 Phase with OPP9 Oxygen Stacking. *Inorg. Chem.* **2011**, *50* (6), 2420–2430. https://doi.org/10.1021/ic102218w.
(26) Biecher, Y.; Smiley, D. L.; Guignard, M.; Fauth, F.; Berthelot, R.; Delmas, C.; Goward, G. R.; Carlier, D. Original Layered OP4-$(Li,Na)_xCoO_2$ Phase: Insights on Its Structure, Electronic Structure, and Dynamics from Solid State NMR. *Inorg. Chem.* **2020**, *58* (8), 5339–5349. https://doi.org/10.1021/acs.inorgchem.9b03417.
(27) Balsys, R. J.; Lindsay Davis, R. The Structure of $Li_{0.43}Na_{0.36}CoO_{1.96}$ Using Neutron Powder Diffraction. *Solid State Ion.* **1994**, *69* (1), 69–74. https://doi.org/10.1016/0167-2738(94)90451-0.
(28) Grey, C. P.; Dupré, N. NMR Studies of Cathode Materials for Lithium-Ion Rechargeable Batteries. *Chem. Rev.* **2004**, *104* (10), 4493–4512. https://doi.org/10.1021/cr020734p.

(29) Pecher, O.; Carretero-González, J.; Griffith, K. J.; Grey, C. P. Materials' Methods: NMR in Battery Research. *Chem. Mater.* **2017**, *29* (1), 213–242. https://doi.org/10.1021/acs.chemmater.6b03183.
(30) Komaba, S.; Ishikawa, T.; Yabuuchi, N.; Murata, W.; Ito, A.; Ohsawa, Y. Fluorinated Ethylene Carbonate as Electrolyte Additive for Rechargeable Na Batteries. *ACS Appl. Mater. Interfaces* **2011**, *3* (11), 4165–4168. https://doi.org/10.1021/am200973k.

(31) Rodríguez-Carvajal, J. Recent Advances in Magnetic Structure Determination by Neutron Powder Diffraction. *Phys. B Condens. Matter* **1993**, *192* (1–2), 55–69. https://doi.org/10.1016/0921-4526(93)90108-I.

(32) Rietveld, H. M. A Profile Refinement Method for Nuclear and Magnetic Structures. *J. Appl. Crystallogr.* **1969**, *2* (2), 65–71. https://doi.org/10.1107/S0021889869006558.
(33) Fauth, F.; Peral, I.; Popescu, C.; Knapp, M. The New Material Science Powder Diffraction Beamline at ALBA Synchrotron. *Powder Diffr.* **2013**, *28* (S2), S360–S370.
(34) Massiot, D.; Fayon, F.; Capron, M.; King, I.; Le Calvé, S.; Alonso, B.; Durand, J.-O.; Bujoli, B.; Gan, Z.; Hoatson, G. Modelling One-and Two-Dimensional Solid-State NMR Spectra. *Magn. Reson. Chem.* **2002**, *40* (1), 70–76. https://doi.org/10.1002/mrc.984.
(35) Zhang, P.; Capaz, R. B.; Cohen, M. L.; Louie, S. G. Theory of Sodium Ordering in Na_xCoO_2. *Phys. Rev. B* **2005**, *71* (15), 153102.
(36) Wang, Y.; Ni, J. Effect of Electronic Correlation on the Na Ordering of Na_xCoO_2. *J. Phys. Condens. Matter* **2007**, *19,* 086203. https://iopscience.iop.org/article/10.1088/0953-8984/19/8/086203
(37) Igarashi, D.; Miyazaki, Y.; Kajitani, T.; Yubuta, K. Disorder-Order Transitions in Na_xCoO_2 ($X \sim 0.58$). *Phys. Rev. B* **2008**, *78* (18), 184112. https://doi.org/10.1103/PhysRevB.78.184112.
(38) Platova, T. A.; Mukhamedshin, I. R.; Alloul, H.; Dooglav, A. V.; Collin, G. Nuclear Quadrupole Resonance and X-Ray Investigation of the Structure of $Na_{2/3}CoO_2$. *Phys. Rev. B* **2009**, *80* (22), 224106. https://doi.org/10.1103/PhysRevB.80.224106.
(39) Yabuuchi, N.; Kajiyama, M.; Iwatate, J.; Nishikawa, H.; Hitomi, S.; Okuyama, R.; Usui, R.; Yamada, Y.; Komaba, S. P2-Type $Na_x[Fe_{1/2}Mn_{1/2}]O_2$ Made from Earth-Abundant Elements for Rechargeable Na Batteries. *Nat. Mater.* **2012**, *11* (6), 512.
(40) Billaud, J.; Singh, G.; Armstrong, A. R.; Gonzalo, E.; Rodattis, V.; Armand, M.; Rojo, T.; Bruce, P. G. $Na_{0.67}Mn_{1-x}Mg_xO_2$ ($0 < X < 0.2$): A High Capacity Cathode for Sodium-Ion Batteries. *Energy Environ. Sci.* **2014**, *7*, 1387.
(41) Mortemard de Boisse, B.; Carlier, D.; Guignard, M.; Bourgeois, L.; Delmas, C. P2-$Na_xMn_{1/2}Fe_{1/2}O_2$ Phase Used as Positive Electrode in Na Batteries: Structural Changes Induced by the Electrochemical (De)intercalation Process. *Inorg. Chem.* **2014**, *53* (20), 11197–11205. https://doi.org/10.1021/ic5017802.
(42) Carlier, D.; Blangero, M.; Ménétrier, M.; Pollet, M.; Doumerc, J.-P.; Delmas, C. Sodium Ion Mobility in $Na_X CoO_2$ ($0.6 < X < 0.75$) Cobaltites Studied by ^{23}Na MAS NMR. *Inorg. Chem.* **2009**, *48* (15), 7018–7025. https://doi.org/10.1021/ic900026c.
(43) Igarashi, D.; Miyazaki, Y.; Yubuta, K.; Kajitani, T. Precise Control of Na Content in the Layered Cobaltate γ-Na_xCoO_2. *J. Electron. Mater.* **2010**, *39* (9), 1669–1673. https://doi.org/10.1007/s11664-010-1238-9.
(44) Clément, R. J.; Billaud, J.; Robert Armstrong, A.; Singh, G.; Rojo, T.; Bruce, P. G.; Grey, C. P. Structurally Stable Mg-Doped P2-$Na_{2/3}Mn_{1-y}Mg_yO_2$ Sodium-Ion Battery Cathodes with High Rate Performance: Insights from Electrochemical, NMR and Diffraction Studies. *Energy Environ. Sci.* **2016**, *9* (10), 3240–3251. https://doi.org/10.1039/C6EE01750A.

(45) Zhang, J.-N.; Li, Q.; Yi, W.; Zheng, J.; Yu, X.; Li, H. Dynamic Evolution of Cathode Electrolyte Interphase (CEI) on High Voltage $LiCoO_2$ Cathode and Its Interaction with Li Anode. *Energy Storage Mater.* **2018**, *14*, 1–7.

(46) Castets, A.; Carlier, D.; Zhang, Y.; Boucher, F.; Ménétrier, M. Multinuclear NMR and DFT Calculations on the $LiFePO_4$·OH and $FePO_4$·H_2O Homeotypic Phases. *J. Phys. Chem. C* **2012**, *116* (34), 18002–18014. https://doi.org/doi.org/10.1021/jp302549s.

(47) Bamine, T.; Boivin, E.; Boucher, F.; Messinger, R. J.; Salager, E.; Deschamps, M.; Masquelier, C.; Croguennec, L.; Ménétrier, M.; Carlier, D. Understanding Local Defects in Li-Ion Battery Electrodes through Combined DFT/NMR Studies: Application to $LiVPO_4F$. *J. Phys. Chem. C* **2017**, *121* (6), 3219–3227. https://doi.org/10.1021/acs.jpcc.6b11747.

(48) Nguyen, L. H.; Sanz Camacho, P.; Broux, T.; Olchowka, J.; Masquelier, C.; Croguennec, L.; Carlier, D. Density Functional Theory-Assisted ^{31}P and ^{23}Na Magic-Angle Spinning Nuclear Magnetic Resonance Study of the $Na_3V_2(PO_4)_2F_3$–$Na_3V_2(PO_4)_2FO_2$ Solid Solution: Unraveling Its Local and Electronic Structures. *Chem. Mater.* **2019**, *31* (23), 9759–9768. https://doi.org/doi.org/10.1021/acs.chemmater.9b03546.

(49) Hinuma, Y.; Meng, Y. S.; Ceder, G. Temperature-Concentration Phase Diagram of P2 -Na_xCoO_2 from First-Principles Calculations. *Phys. Rev. B* **2008**, *77* (22), 224111. https://doi.org/10.1103/PhysRevB.77.224111.

TOC

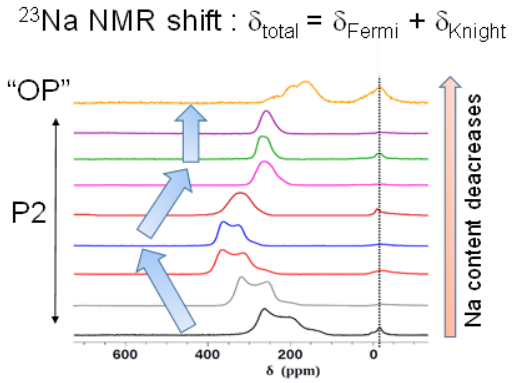
^{23}Na NMR shift : $\delta_{total} = \delta_{Fermi} + \delta_{Knight}$
"OP"
P2
Na content deacreases
600
400
200
0
δ (ppm)